New Phytologist

Plant functional traits and canopy structure control the relationship between photosynthetic CO_2 uptake and far-red sun-induced fluorescence in a Mediterranean grassland under different nutrient availability

Mirco Migliavacca[1], Oscar Perez-Priego[1], Micol Rossini[2], Tarek S. El-Madany[1], Gerardo Moreno[3], Christiaan van der Tol[4], Uwe Rascher[5], Anna Berninger[1], Verena Bessenbacher[1], Andreas Burkart[5], Arnaud Carrara[6], Francesco Fava[7], Jin-Hong Guan[1,8], Tiana W. Hammer[1], Kathrin Henkel[1], Enrique Juarez-Alcalde[3], Tommaso Julitta[2], Olaf Kolle[1], M. Pilar Martín[9], Talie Musavi[1], Javier Pacheco-Labrador[9], Andrea Pérez-Burgueño[3], Thomas Wutzler[1], Sönke Zaehle[1] and Markus Reichstein[1]

[1]Max Planck Institute for Biogeochemistry, Hans Knöll Straße 10, Jena D-07745, Germany; [2]University of Milano Bicocca, Piazza della Scienza 1, Milan 20126, Italy; [3]INDEHESA-Forest Research Group, Universidad de Extremadura, Plasencia 10600, Spain; [4]Department of Water Resources, Faculty of Geo-Information Science and Earth Observation (ITC), University of Twente, Enschede 7500 AE, the Netherlands; [5]Institute of Bio- and Geosciences, IBG-2: Plant Sciences, Forschungszentrum Jülich GmbH, Leo-Brandt-Str., Jülich 52425, Germany; [6]Fundación Centro de Estudios Ambientales del Mediterráneo (CEAM), Valencia 46980, Spain; [7]International Livestock Research Institute, Naivasha Rd, Nairobi 30709, Kenya; [8]State Key Laboratory of Soil Erosion and Dryland Farming on Loess Plateau, Northwest A&F University, Yangling Shaanxi 712100, China; [9]Environmental Remote Sensing and Spectroscopy Laboratory (SpecLab), Institute of Economics, Geography and Demography (IEGD), Spanish National Research Council (CSIC), Albasanz 26-28, Madrid 28037, Spain

Author for correspondence:
Mirco Migliavacca
Tel: +493641576281
Email: mmiglia@bgc-jena.mpg.de

Received: *6 October 2016*
Accepted: *8 December 2016*

New Phytologist (2017) **214:** 1078–1091
doi: 10.1111/nph.14437

Key words: canopy structure, far-red sun-induced fluorescence, functional traits, gross primary productivity (GPP), leaf inclination distribution function, nutrient manipulation, soil–canopy observation of photosynthesis and energy (SCOPE) model.

Summary

- Sun-induced fluorescence (SIF) in the far-red region provides a new noninvasive measurement approach that has the potential to quantify dynamic changes in light-use efficiency and gross primary production (GPP). However, the mechanistic link between GPP and SIF is not completely understood.
- We analyzed the structural and functional factors controlling the emission of SIF at 760 nm (F_{760}) in a Mediterranean grassland manipulated with nutrient addition of nitrogen (N), phosphorous (P) or nitrogen–phosphorous (NP). Using the soil–canopy observation of photosynthesis and energy (SCOPE) model, we investigated how nutrient-induced changes in canopy structure (i.e. changes in plant forms abundance that influence leaf inclination distribution function, LIDF) and functional traits (e.g. N content in dry mass of leaves, N%, Chlorophyll *a+b* concentration (*C*ab) and maximum carboxylation capacity (V_{cmax})) affected the observed linear relationship between F_{760} and GPP.
- We conclude that the addition of nutrients imposed a change in the abundance of different plant forms and biochemistry of the canopy that controls F_{760}. Changes in canopy structure mainly control the GPP–F_{760} relationship, with a secondary effect of *C*ab and V_{cmax}.
- In order to exploit F_{760} data to model GPP at the global/regional scale, canopy structural variability, biodiversity and functional traits are important factors that have to be considered.

Introduction

Photosynthetic CO_2 uptake by terrestrial ecosystems is a key process controlling the variability of the global carbon (C) cycle (Beer *et al.*, 2010) and provides ecosystem services that are essential for human well-being (including food, fiber, energy and oxygen). In the last several decades, the development of eddy covariance technique networks and chamber measurements have increased the number of estimates of ecosystem-scale gross primary production (GPP). These data have been used to develop upscaling methods ranging from purely data-driven approaches (Jung *et al.*, 2011) to process-based estimates (Beer *et al.*, 2010), which provide regional and global estimates of GPP. One of the most widely used methods to upscale GPP relies on the use of remote sensing information describing ecosystem structure and light use efficiency (LUE), together with climate variables through a modeling approach (e.g. Heinsch *et al.*, 2006).

Remote sensing based measurements of sun-induced chlorophyll fluorescence are opening new possibilities to estimate GPP directly (Beer *et al.*, 2010; Guanter *et al.*, 2013; Zhang *et al.*, 2014; Yang *et al.*, 2015). Recent studies showed that sun-induced fluorescence (SIF) can track changes in LUE, and therefore can

© 2017 The Authors
New Phytologist © 2017 New Phytologist Trust

be directly linked to GPP at a variety of scales, from leaves (Meroni *et al.*, 2008) and ecosystem (Damm *et al.*, 2010; Rossini *et al.*, 2010), to regional and global (Lee *et al.*, 2013; Guanter *et al.*, 2014; Parazoo *et al.*, 2014; Zhang *et al.*, 2016).

The assumption for the use of SIF to predict GPP is that under natural illumination conditions the amount of chlorophyll fluorescence emitted by vegetation scales directly with the amount of light that is absorbed by the active photosynthetic tissues, the amount of Chlorophyll *a*+*b* (*C*ab) and with photosynthetic efficiency. Sun-induced fluorescence emitted by a plant is a small fraction of the radiation reflected in the red (*c.* 685 nm) and near-infrared spectral regions (*c.* 740 nm), but is typically estimated (F_{760}) exploiting the telluric oxygen absorption band (Meroni *et al.*, 2009). Recent studies and technological development of high-resolution spectrometers and field spectroscopy techniques have allowed the estimation of SIF in the proximity of the red region (685 nm), but the uncertainty of the retrieval is still high (Cogliati *et al.*, 2015). Other studies showed that F_{760} includes information about photosynthetic efficiency, canopy structure and absorbed photosynthetically active radiation (APAR) (Guanter *et al.*, 2012; Yang *et al.*, 2015), whereas SIF in the red region is more closely linked to photosynthetic efficiency and activity of the photosystem II (Porcar-Castell *et al.*, 2014).

Recently, F_{760} estimates have been proposed to directly predict GPP using plant functional type-specific linear relationships, or modified versions of LUE models (Rossini *et al.*, 2015; Wieneke *et al.*, 2016). However, both modeling studies (Damm *et al.*, 2015) and empirical evidence (Perez-Priego *et al.*, 2015; Wieneke *et al.*, 2016) showed that depending on the spatial (leaf vs canopy) and temporal (sub daily vs daily or weekly) scales at which F_{760} was observed, the functional relationship GPP–F_{760} may be nonlinear, and the sensitivity of GPP to variations of F_{760} was variable across and within plant functional types.

Damm *et al.* (2015) showed that the asymptotic leaf-level relationship observed between F_{760} and GPP became more linear at the ecosystem scale and with coarser temporal aggregation. By using a radiative transfer model, the authors also identified a series of factors affecting the GPP–F_{760} relationship such as the variability in leaf area index (LAI), fraction of nonphotosynthetic vegetation components, foliar biochemistry (*C*ab, and maximum carboxylation capacity, V_{cmax}), and leaf inclination distribution function (LIDF) parameters LIDFa and LIDFb. The latter are important parameters describing the distribution of leaf inclination within the canopy, which determines the transmission and reflection of radiation by vegetation canopies: LIDFa is the average leaf inclination, whereas LIDFb determines the bimodality of the distribution (Verhoef, 1984).

A linear relationship between GPP and F_{760} was also found in a fully factorial nutrient fertilization experiment conducted in a Mediterranean grassland (Perez-Priego *et al.*, 2015). The authors found a statistical differences in the slope and intercept of the GPP–F_{760} relationship and a variable slope across treatments. This suggested that regulatory mechanisms related to the nitrogen (N) and phosphorous addition might have reduced the degree of coupling between fluorescence and photosynthesis (P) (e.g. Porcar-Castell *et al.*, 2014). Similar conclusions were drawn by Cendrero-Mateo *et al.* (2016) in a N and water manipulation study conducted on camelina and wheat.

One current challenge is to understand the mechanisms controlling the relationship GPP–F_{760}, or more generally GPP and SIF, for which many hypotheses have been proposed (Guanter *et al.*, 2014; Damm *et al.*, 2015; Liu *et al.*, 2017).

First, changes in the sensitivity of SIF to photosynthesis rates can be due to competition between the three processes involved in the dissipation of absorbed light: photochemistry (i.e. reactions involved in the photosynthesis), radiative energy losses (i.e. fluorescence emissions) and nonradiative energy dissipation (i.e. nonphotochemical quenching, NPQ) (van der Tol *et al.*, 2009a; Porcar-Castell *et al.*, 2014; van der Tol *et al.*, 2015). For instance Cendrero-Mateo *et al.* (2016) showed that under acute water stress the modulation between NPQ and SIF controlled the functional relationship between CO_2 uptake and SIF. Second, canopy structure (LAI and LIDF among all) affects the light quality and regimes within the canopy, which controls the distribution and size of pools of carotenoids involved in the xanthophyll cycle. This in return affects the rates of NPQ and the ratio between radiative and nonradiative dissipation of energy (Niinemets *et al.*, 2003). Third, multiple scattering and reabsorption of emitted SIF within the canopy depends also on vegetation structure (Fournier *et al.*, 2012; Knyazikhin *et al.*, 2013; Damm *et al.*, 2015), which affects the GPP–F_{760} relationship by controlling the ratio of photons reabsorbed or escaping the canopy. Finally, Cendrero-Mateo *et al.* (2016) highlighted the importance of nutrient availability and showed that when N is a limiting factor, functional traits (e.g. *C*ab) modulate the slope of the relationship between GPP and SIF.

In this study we investigated the structural and physiological factors controlling the relationship between F_{760} and GPP in a Mediterranean grassland subject to differing nutrient availability induced by fertilization.

We hypothesized that the observed changes in the relationship between F_{760} and GPP were related to changes in some functional traits (changes in plant N and P content per g dry mass (N % and P%, respectively), V_{cmax} and *C*ab) caused by the application of the fertilization, and changes in canopy structure (LIDFa and LIDFb) due to changes in the composition of the main plant forms (i.e. grasses, forbs and legumes) induced by both direct (e.g. competition between plant forms) and indirect (i.e. selective grazing) effects of fertilization.

The main objective was to identify how the variability in canopy structure (LIDFa, LIDFb), and functional traits (e.g. N %, *C*ab and V_{cmax}) induced by different fertilization treatments controlled the functional relationship between GPP and F_{760}.

In particular we focused on the following two questions: How do observed changes in canopy structure and functional traits affect the F_{760} signal? And why does the relationship between GPP and F_{760} change across treatments?

In order to test the different hypotheses, we combined near-simultaneous estimates of F_{760} obtained using narrow band spectrometers, and GPP obtained with manual transparent and opaque chamber measurements, with the soil–canopy

© 2017 The Authors
New Phytologist © 2017 New Phytologist Trust

observation of photosynthesis and the energy balance (SCOPE) radiative transfer model (van der Tol *et al.*, 2009b). We performed a factorial modeling experiment with SCOPE to attempt to disentangle the main drivers (canopy structure vs functional traits) of F_{760} and to understand the factors controlling GPP–F_{760} relationship.

Materials and Methods

Experimental site and set-up

The study was conducted in a Mediterranean savannah located in Spain (39°56′24.68″N, 5°45′50.27″W; Majadas de Tietar, Caceres), characterized as a continental Mediterranean climate, with temperate winters and warm dry summers. The mean annual temperature is 16.7°C and the mean annual precipitation is *c.* 700 mm distributed mainly between September and May, with large interannual variations.

The site is managed as a typical wood pasture (*Iberian Dehesa*) with low-intensity grazing by cows (< 0.3 cows ha^{-1}). The vegetation is dominated by an herbaceous stratum, and by a sparse tree layer with low density of oak trees (mostly *Quercus Ilex* (L.), *c.* 20 trees ha^{-1}). The herbaceous stratum is dominated by species of the three main functional plant forms: grasses, forbs and legumes (e.g. *Tolpis barbata*, *Anthoxanthum aristatum*, *Ornithopus compressus*, *Trifolum striatum*, *Lotus parviflorus* and *Plantago lagopus*).

At the site we established a small-scale manipulation experiment focused on the herbaceous layer (Perez-Priego *et al.*, 2015), which consisted of four 20 × 20 m randomized blocks. Within each block we established four plots of 9 × 9 m with 2 m of buffer between treatments (Supporting Information Fig. S1). We manipulated each plot as follows: control treatment (C) with no fertilization; nitrogen addition (N) with one application of 100 kg N ha^{-1} as potassium nitrate (KNO_3) and ammonium nitrate (NH_4NO_3); phosphorous addition (P) with 50 kg P ha^{-1} as monopotassium phosphate (KH_2PO_4); and nitrogen–phosphorous addition (NP), 100 kg N ha^{-1} and 50 kg P ha^{-1} as ammonium nitrate (NH_4NO_3) and monopotassium phosphate (KH_2PO_4). Approximately 2 l m^{-2} of water was added to the C plots to compensate for the liquid fertilization applied in the N, NP and P treatments.

CO_2 flux measurements with transparent and opaque chambers (i.e. net ecosystem CO_2 exchange (NEE) and daytime ecosystem respiration (R_{eco})) and spectral measurements were conducted nearly simultaneously in a 60 × 60 cm collar within each plot, for a total of 16 samples for each field campaign.

Flux and spectral measurements were carried out in four field campaigns: campaign 1 – before fertilization (20 March 2014); campaign 2 – 3 wk after fertilization (15 April 2014) during the peak of the growing period; campaign 3 – at the beginning of the senescence period (7 May 2014); and campaign 4 – during the dry period (27 May 2014).

Ancillary measurements and plant traits were collected during each field campaign: LAI, aboveground biomass and leaf mass per area (LMA) were directly (i.e. destructive sampling) measured in four parcels (0.25 × 0.25 m) within each plot. The abundance of each functional group (fraction of grass, forbs and legumes) and green to dry biomass ratio also were determined. Carbon concentration (C%), N% and P% were determined as described in detail in Perez-Priego *et al.* (2015).

Field spectroscopy and sun-induced fluorescence retrieval

Top-of-canopy spectral radiances were collected at midday (between 11:00 h and 15:00 h local solar time) under clear-sky conditions at each plot before the flux measurements. Two portable spectrometers (HR4000; OceanOptics, Dunedin, FL, USA) characterized by different spectral resolutions were used: spectrometer 1, characterized by a full width at half maximum (FWHM) of 0.1 nm covering the spectral range of 700–800 nm, was specifically designed for the estimation of sun-induced chlorophyll fluorescence at the O_2-A absorption band (at 760 nm) (F_{760}); spectrometer 2 (FWHM = 1 nm, 400–1000 nm spectral range) was used for the computation of reflectance and vegetation indices. Spectrometers were housed in a thermally regulated Peltier box, keeping the internal temperature at 25°C in order to reduce dark current drift. The spectrometers were spectrally calibrated with a source of known characteristics (CAL-2000 mercury argon lamp; OceanOptics), whereas the radiometric calibration was inferred from cross-calibration measurements performed with a FieldSpec FR Pro spectrometer (ASD FIeldspec, Boulder, CO, USA) regularly calibrated by the manufacturer. Incident solar irradiance was measured by nadir observations of a leveled calibrated standard 99% reflectance panel (Spectralon; LabSphere, North Sutton, NH, USA).

Measurements were acquired using bare fiber optics with an angular field of view of 25°. The average canopy plane was observed from nadir at a distance of 110 cm (43 cm diameter field of view) allowing for measurement collection of the surface area covered by the chamber measurements. Five measurements were collected for each plot according to Perez-Priego *et al.* (2015).

Spectral data were acquired with dedicated software (Meroni & Colombo, 2009) and processed with a specifically developed IDL (ITTVIS IDL 7.1.1) application. This application allowed the basic processing steps of raw digital numbers necessary for the computation of the hemispherical conical reflectance factor (Meroni *et al.*, 2011).

Sun-induced fluorescence (SIF) was estimated by exploiting the spectral fitting method (Meroni *et al.*, 2010), assuming linear variation of the reflectance and fluorescence in the O_2-A absorption band region *c.* 760 nm, and referred to as F_{760}. The spectral interval used for SIF estimation was set to 759.00–767.76 nm for a total of 439 spectral channels used.

The normalized difference vegetation index (NDVI) from the measured top of the canopy reflectance also was computed using the smoothed reflectance spectra observed at 800 nm wavelength in the near-infrared region and 680 nm in the red region.

© 2017 The Authors
New Phytologist © 2017 New Phytologist Trust

Gross primary productivity estimated with manual chambers

Net ecosystem CO_2 exchange (NEE) fluxes were measured with three nonsteady-state flow-through type transparent chambers of (60 × 60 × 60 cm). The systems were equipped with an infrared gas analyzer (IRGA LI-840; Li-Cor, Lincoln, NE, USA), which measures CO_2 and water vapor mole fractions (W) at 1 Hz. A series of environmental and soil measurements also were collected: photosynthetically active radiation (PAR) was measured with a quantum sensor (Li-190; Li-Cor) mounted outside the chamber so that it could be handled and leveled; air temperature was measured with a thermistor probe (T_a, type 107; Campbell Scientific, Logan, UT, USA); soil water content was determined with an impedance soil moisture probe (Theta Probe ML2x; Delta-T Devices, Cambridge, UK) at 5 cm depth. Vapor pressure deficit (VPD) was computed using relative humidity measurements and T_a (Campbell & Norman, 1998). Net radiation of the grass was measured at the nearby eddy covariance station with a four-channel net radiometer (CNR4; Kipp&Zonen, Delft, the Netherlands).

For the NEE measurement, the transparent chamber was placed on the collar (closed position for at least 3 min), and fluxes were calculated from the rate of change in the CO_2 molar fraction (referenced to dry air) within the chamber. A similar procedure was carried out for respiration measurements (R_{eco}), but using an opaque blanket that covered the entire chamber to keep dark during the measurements. Chamber disturbance effects and correction for systematic and random errors (i.e. leakage, water dilution, gas density correction and light attenuation by the chamber wall) were applied according to Perez-Priego *et al.* (2015). Fluxes and associated uncertainties were calculated with a self-developed open-source R package (http://r-forge.r-project.org/projects/respchamberproc/). GPP was computed as the difference between R_{eco} and NEE measurements taken consecutively with the chambers. The dataset is available on request from the corresponding author.

Modeling SIF at 760 nm and GPP

The coupled fluorescence–photosynthesis model SCOPE is a vertical (1D) integrated radiative transfer and energy balance model that simulates photosynthesis, radiative transfer in the leaf and canopy, SIF for both emission peaks, and the surface energy balance (van der Tol *et al.*, 2009a, 2014). SCOPE was used recently in a series of studies linking SIF and photosynthesis at different scales (Zhang *et al.*, 2014; Damm *et al.*, 2015; Verrelst *et al.*, 2015).

SCOPE combines a number of radiative transfer models (RTM): one for the leaf Fluspect (Vilfan *et al.*, 2016) and three for the canopy: RTMo, RTMt and RTMf (van der Tol *et al.*, 2009b). Fluspect is an extension of the widely used PROSPECT model (Jacquemoud & Baret, 1990), which simulates the radiative transfer of incident light and emitted fluorescence within the leaf. The outputs are the reflectance and transmittance spectra, and the probability that an incident photon of wavelength λ_i is emitted as fluorescence at wavelength λ_j at either side of the leaf.

The three radiative transfer modules for the canopy are all based on the scattering of arbitrarily inclined leaves (SAIL) model (Verhoef, 1984). They treat the vegetation in a stochastic way with 60 elementary layers, 13 discrete leaf zenith inclination and 36 leaf azimuth classes. LIDF, provided as input, describes the probability of a leaf to belong a zenith inclination class, but the leaf azimuth angle distribution is assumed to be uniform. The leaf zenith inclination is provided either as a histogram of probabilities per class (from horizontal to vertical), or by means of two parameters, LIDFa and LIDFb, which together describe the cumulative leaf inclination distribution as a continuously rising function of zenith angle. LIDFa determines the average leaf inclination, whereas LIDFb determines the bimodality of the distribution.

The distribution of solar irradiance over leaves in the canopy is simulated with the model RTMo: a four-stream radiative transfer model. The four simulated fluxes include direct, diffuse upward, diffuse downward and flux in the observation direction.

A routine for photochemical quenching (PQ) and NPQ of the fluorescence are used together with the output of the Fluspect model to simulate the SIF emission per leaf angle and leaf layer. The emitted fluorescence then is used in the module RTMf, which simulates scattering and absorption of SIF within the canopy. The biochemical model for PQ and NPQ requires leaf temperatures as input, calculated from the energy balance module and the RTMt module for radiative transfer of thermal radiation. SCOPE includes a number of biochemical routines for PQ and NPQ. In this study we used the model of van der Tol *et al.* (2014), which is a combination of a photosynthesis exchange models for C_3 and C_4 vegetation (Collatz *et al.*, 1991, 1992), the gas exchange model of Ball–Berry model, and an empirical parameterization of the relationship between PQ and NPQ. We selected the parameterization calibrated from data as provided in van der Tol *et al.* (2014).

In order to simulate photosynthesis and fluorescence, SCOPE requires a series of meteorological forcing (incoming shortwave and longwave radiation, T_a, relative humidity, wind speed and CO_2 concentration) and four classes of parameters: vegetation structure parameters, such as canopy height, LIDFa, LIDFb and LAI; leaf biophysical parameters: *C*ab, carotenoids, dry matter content (C_{dm}), leaf equivalent water thickness (C_w), senescent material (C_s); optical parameters: reflectance of soil in the visible, near-infrared and thermal bands, and vegetation (thermal) emissivity; and plant physiological parameters: stomatal conductance parameter (m), V_{cmax} of a top leaf standardized to a reference temperature at 25°C.

SCOPE model simulations set up

SCOPE meteorological inputs were measured along with chambers measurements. When the meteorological inputs data were not available, gap-filling using the linear interpolation of two consecutive measurements collected at the nearby eddy covariance flux tower at 10 min of temporal resolution was applied. The solar zenith angle at the time of the collection of the spectral measurements was used as model input.

© 2017 The Authors
New Phytologist © 2017 New Phytologist Trust

New Phytologist

Table 1 List of parameters used for soil–canopy observation of photosynthesis and energy (SCOPE) model simulations

Parameters	Symbol	Units	Range	Parameterization	Source
Chlorophyll *a*+*b* content	*C*ab	μg cm^{-2}	35.94–56.53	Variable	From field observations N%, P% and LMA
Maximum carboxylation capacity	V_{cmax}	μmol m^{-2} s^{-1}	54.26–88.59	Variable	From field observations N%, P% and LMA
Leaf equivalent water thickness	*C* w	cm	0.009	Fixed	Literature
Leaf angle distribution parameter *a*	LIDFa	/	−1 to −0.37	Variable	Computed from inversion of LIDF model (#Method)
Leaf angle distribution parameter *b*	LIDFb	/	−0.14 to 0	Variable	Computed from inversion of LIDF model (#Method)
Leaf width	*W*	m	0.01	Fixed	Literature
Ball–Berry stomatal conductance parameter	*M*	/	8	Fixed	Literature
Dark respiration rate at 25°C as fraction of V_{cmax}	*R* d	/	0.015	Fixed	Literature
Leaf area index	LAI	/	0.44–2.46	Variable – Prescribed	Field observations
Canopy height	h_c	m	0.05–0.20	Variable – Prescribed	Field observations

N%, total nitrogen content in leaves; P%, total phosphorous content in leaves; LMA, leaf mass per unit area.

The model was parameterized using the structural and functional traits derived from the field sampling as described in Table 1.

For each individual run LAI, canopy height, *C*ab, C_{dm}, V_{cmax}, LIDFa and LIDFb parameters were estimated for each plot and used to parameterize the model. Canopy height was estimated in the field with a meter stick in five positions within the measurement collar. For the other parameters we used data from the literature for C_3 grasses (Table 1). Soil reflectance spectra were collected in a dedicated field campaign in April 2015 and used for all the runs.

In order to evaluate the effects of fertilized-induced changes in functional traits (*C*ab, V_{cmax}) and canopy structure (specifically LIDFa, LIDFb) on the simulated F_{760} signal and on the GPP–F_{760} relationship, we performed a factorial modeling experiment with four cases. In all cases, the parameters varied in time (i.e. between field campaigns) to account for phenology. RUN REFERENCE: LIDFa, LIDFb, V_{cmax} and *C*ab fixed across treatments to the mean estimates of the C treatment; RUN TRAITS: V_{cmax} and *C*ab variable across treatments to account for differences in functional traits induced by fertilization. LIDFa and LIDFb fixed across treatments, only variable in time; RUN STRUCT: LIDFa and LIDFb variable across treatments to account for differences in canopy structure induced by changes in composition of plant forms after the fertilization. V_{cmax} and *C*ab fixed across treatments, only variable in time; RUN TRAITS–STRUCT: both structural parameters (LIDFa, LIDFb) and traits (V_{cmax} and *C*ab) variable across treatments.

It should be noted that the values of LAI, canopy height and important structural properties of the canopy were prescribed using data measured in the field campaigns.

A schematic representation of the modeling experiment and the four different cases is reported in Fig. S2.

Each run of SCOPE was performed to simulate GPP, top-of-canopy reflectance, and F_{760} for each measurement time and for each plot for a total of 64 runs for each case (16 runs for each field campaign). To match the F_{760} estimated from field measurements the model values of fluorescence at the 760 nm wavelengths were used.

The parameters *C*ab and V_{cmax} were determined for each plot and each field campaign from N%, P% and LMA measurements using four different approaches described in Methods S1.

The results presented in the following are obtained using a parameterization of V_{cmax}-derived fitting the empirical relationship between total N% and V_{cmax} obtained using data from Feng & DIetze (2013) and Walker *et al.* (2014) for herbaceous species ($R^2 = 0.29$, $P < 0.01$):

$$V_{cmax} = 49.57 \cdot \log_e(N\%) + 45.57 \quad \text{Eqn 1}$$

*C*ab was parameterized using the empirical relationship with V_{cmax} proposed by Houborg *et al.* (2013) for C_3 plants:

$$Cab = \left(\frac{V\text{cmax} - b}{a}\right) \quad \text{Eqn 2}$$

where $b = -27.34$ and $a = 2.529$. In this equation, *C*ab is expressed in μg cm^{-2} and V_{cmax} in μmol m^{-2} s^{-1}.

We also tested an additional parameterization of V_{cmax} and *C*ab, which were derived from N% content weighted by the green fraction of the vegetation (Fig. S3).

The parameters LIDFa and LIDFb were estimated for each field plot and each field campaign as follows: first, we assumed a characteristic LIDF for grass (erectophile, LIDFa = −1 LIDFb = 0), forbs (spherical LIDFa = −0.35 LIDFb = −0.15) and legumes (planophile LIDFa = 1 LIDFb = 0) according to the literature (Wohlfahrt *et al.*, 2001; Barillot *et al.*, 2011); secondly, we computed the cumulative weighted mean LIDF (cwLIDF) as the mean of the individual LIDF for each plant form weighted by its abundance; finally, the parameters LIDFa and LIDFb were estimated by inverting the LIDF model included in SCOPE against the cwLIDF. Parameters were estimated by minimizing the residuals-sum-of-squares between simulated and observed cwLIDF using a quasi-Newton algorithm, which allows box-

© 2017 The Authors
New Phytologist © 2017 New Phytologist Trust

constraints (Byrd *et al.*, 1995). An example of the LIDF function obtained with the proposed method is reported in the Fig. S4.

The impact of using different LIDF assumptions on reflectance and SIF simulated with SCOPE was also tested. In Fig. S5 we presented SCOPE simulations of reflectance and SIF for three LIDF: planophile, erectophile and spherical, assuming constant LAI to 1.0 $m^2\,m^{-2}$, V_{cmax} to 60 $\mu mol\,m^{-2}\,s^{-1}$ and *C*ab to 30 $\mu g\,cm^{-2}$.

Model evaluation and statistical analysis

The accuracy of F_{760} and GPP simulated with SCOPE was evaluated by computing the Pearson's correlation coefficient (r), mean absolute error (MAE), modeling efficiency (MEF), root mean-squared error (RMSE), the determination coefficient (R^2), and the slope and intercept of the linear regression between observed and modeled data according to Janssen & Heuberger (1995). The statistics were computed for each case using the whole dataset, but also individually by campaign, removing the confounding factor introduced by phenology, and by treatment.

Finally, the parameters of the linear regression between GPP and F_{760} and its variability between treatments was computed for the observed and modeled data (GPP_{SCOPE}, $F_{760SCOPE}$).

Results

Observed fluxes, traits and F_{760}

The time series of treatment mean GPP, F_{760}, N%, LAI of the green fraction of the vegetation, V_{cmax}, *C*ab and the main meteorological variables are reported in Fig. 1 and Table 2. A clear effect of fertilization on functional traits is observed at each campaign. For GPP, LAI and F_{760}, the differences are evident at the peak of the growing season, whereas the differences are minimized during the dry period. The differences between N-fertilized plots and C observed in F_{760} during the last field campaign are significant. Similar differences are observed also in N%, V_{cmax} and *C*ab.

In Table 2, the main meteorological parameters measured during the field campaign and those required to drive SCOPE are reported. Observed changes in plant form abundances (forbs, legumes and grasses) show an increase of the abundance of grasses in contrast to a decrease of forb abundance in N-fertilized plots. Legumes gradually decrease with time, in particular in the N-fertilized plots.

Performance evaluation of SCOPE simulations

SCOPE simulations better reproduce measured F_{760} when variable functional traits and canopy structure are used as inputs for the model runs (Fig. 2). The F_{760} simulated with Run Reference explains only 27% of the variance in the observed values, whereas the Run Traits–Structure explains 61%. In particular, introducing the specific description of the LIDF parameters (LIDFa, LIDFb) for each treatment reduces the systematic bias between model and observation compared with the Run Reference (Table 3; Fig. 2a,c). The slope of the observed vs modeled linear regression decreases from 1.17 (Run Reference) to 1.06 (Run Structure). The importance of the canopy structure is highlighted in Fig. S5: the total emitted flux (sum of all leaves), and the hemispherically integrated flux that escapes the canopy, are the highest for planophile and lowest for erectophile vegetation (Fig. S5a,b). The difference between these three fluxes appears much larger when looking at the vegetation from nadir, as in the experimental set-up (Fig. S5d).

The effect of the variable parameterization of traits (V_{cmax} and *C*ab) is described mainly by the changes in the explained variance of F_{760} modeled, with an increase in the R^2 from 0.56 (Run Structure) to 0.61 (Run Traits–Structure). The use of the SCOPE model inputs specific for each treatment improves both the accuracy of the simulated reflectance and the derived vegetation indices compared with the Run Reference as indicated by the evaluation of simulated NDVI (Fig. S6). The reflectance spectra simulated with the Run Traits–Structure and those measured are presented in Figs S7 and S8. The evaluation conducted by field campaigns (Fig. 3a) and by treatments (Fig. 3b) shows a systematic improvement (i.e. decrease of MAE) with the Run Traits and Run Traits–Structure. The decrease of MAE is larger for campaign 2 (15 April), at the peak of the growing season, when the effect of fertilization on both GPP and F_{760} is observed in N-fertilization treatments. The Run Traits–Structure shows in general lowest MAE and better performances at each campaign and for each treatment.

GPP simulated with SCOPE shows a good agreement with GPP estimated with the chambers (Fig. 4) without systematic differences introduced by the different parameterizations of functional traits and LIDF. Overall, the GPP simulated with SCOPE Run Traits–Structure explains 71–79% of the variance of the observed GPP. In general, SCOPE slightly overestimates the observed GPP, with a slope of the linear regression observed vs modeled of 0.84 for the Run Traits–Structure. This overestimation is likely related to the parameterization of V_{cmax}, a parameter that controls strongly GPP and not F_{760} at canopy level (e.g. Verrelst *et al.*, 2016), applied in this study, which is based on literature. An additional test to evaluate the effects of a variable parameterization of V_{cmax} and *C*ab was conducted by prescribing the LIDF to spherical, which is the typical distribution function used in herbaceous canopies in the literature. Results showed the importance of a variable parameterization of functional traits for simulating F_{760} (Fig. S9).

Evaluation of the GPP–F_{760} relationship and model benchmarking

Figure 5 shows the relationship between GPP and F_{760} observed and modeled with the four modeled cases (Fig. 5a), and the relationship between F_{760} and LAI (Fig. 5b). Results show a better agreement between the observed and modeled relationships of GPP–F_{760} for the Run Traits–Structure, the latter being closer to the observed relationship. The overall higher slope of the simulated results (13.75% compared with the observations) is mainly

© 2017 The Authors
New Phytologist © 2017 New Phytologist Trust

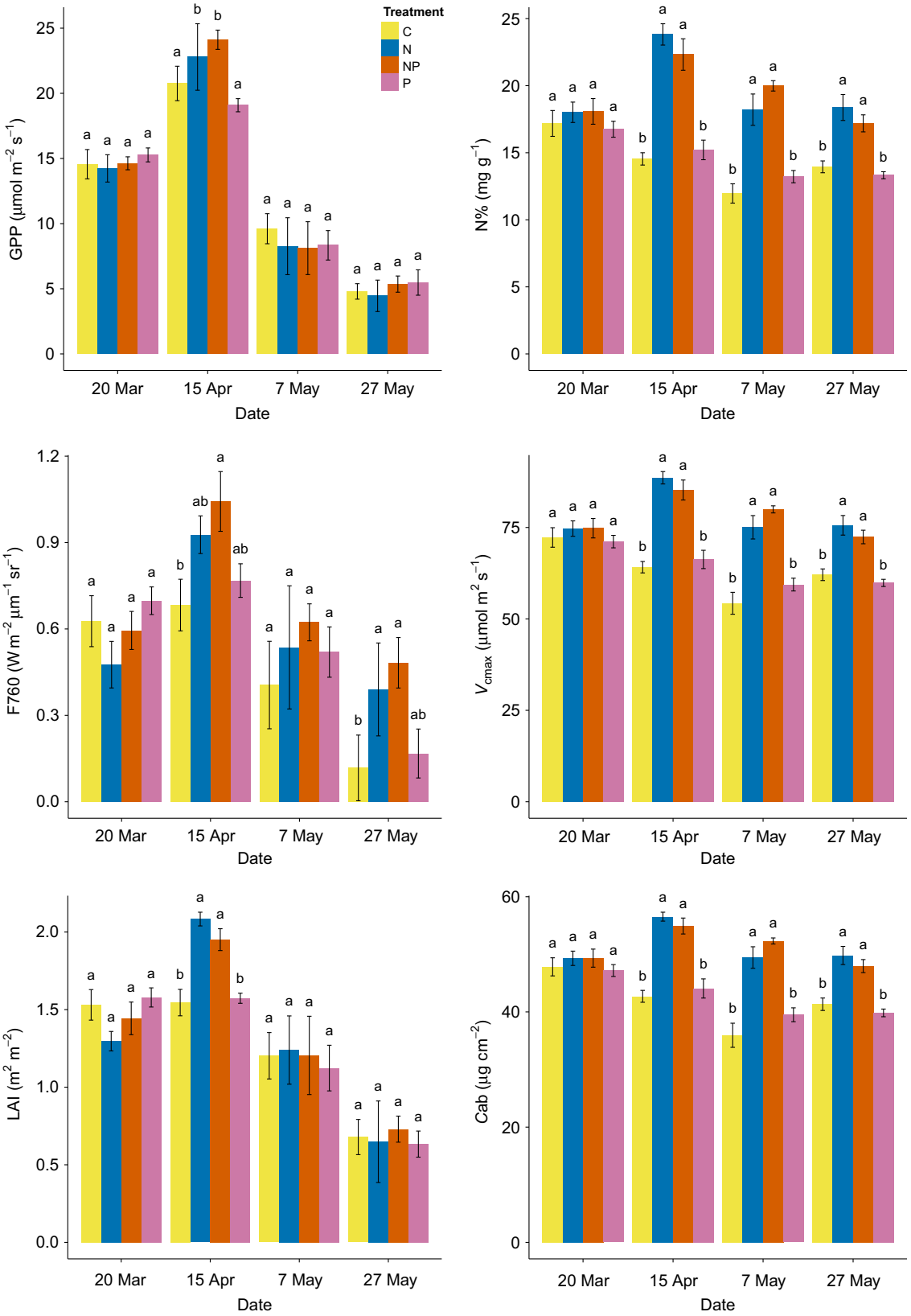

Fig. 1 Seasonal time course of mean midday gross primary productivity (GPP), nitrogen (N) canopy content per g dry mass (N%), fluorescence emission at 760 nm (F_{760}), leaf area index (LAI), derived Chlorophyll *a*+*b* (Cab) and maximum carboxylation capacity (V_{cmax}) among carbon (C), N, nitrogen–phosphorous (NP) and P addition treatments in a Mediterranean grassland. Bars indicate ± SD, $n = 4$. Different letters denote significant difference between treatments (Tukey Honest Significant Difference test, $P < 0.05$).

© 2017 The Authors
New Phytologist © 2017 New Phytologist Trust

Table 2 Ancillary data measured during the field campaign

Campaign	Treatment	N% (mg g^{-1})	SD (mg g^{-1})	Plant forms abundance			PAR (Wm^{-2})	VPD (hPa)	Tair (°C)	SWC (%)
				Forbs (%)	Grass (%)	Legumes (%)				
1	C	17.19	1.92	35.5	56.8	7.7	724.2	12.59	24.06	19.01
20 March 2014	N	18.02	1.52	39.2	45.1	15.0				
	NP	18.08	1.91	29.1	54.3	12.9				
	P	16.75	1.19	26.6	66.6	6.9				
2	C	14.54	0.91	14.5	85.2	0.3	823.4	15.12	29.49	22.58
15 April 2014	N	23.82	1.59	11.9	87.6	0.4				
	NP	22.32	2.34	4.1	95.6	0.3				
	P	15.21	1.46	14.2	85.7	0.1				
3	C	11.96	1.44	43.0	55.1	1.9	650.8	22.40	33.31	4.783
7 May 2014	N	18.21	2.36	28.3	70.7	1.0				
	NP	19.99	0.77	27.2	71.8	1.0				
	P	13.22	0.91	39.5	58.5	2.0				
4	C	13.95	0.88	66.7	33.3	0.0	647.5	15.83	27.68	6.569
27 May 2014	N	18.37	1.94	36.4	63.6	0.0				
	NP	17.19	1.26	40.6	59.4	0.0				
	P	13.32	0.53	56.1	43.9	0.0				

Mean meteorological data measured during each field campaigns are also reported. N%, mean nitrogen content per treatment; Plant forms abundance, mean abundance of plant forms expressed as fraction of leaf area index in different plant forms and reported for each campaign and treatment. PAR, photosynthetically active radiation; VPD, vapor pressure deficit; Tair, air temperature; SWC, soil water content; addition treatments: C, carbon; N, nitrogen; NP, nitrogen–phosphorous; P, phosphorus.

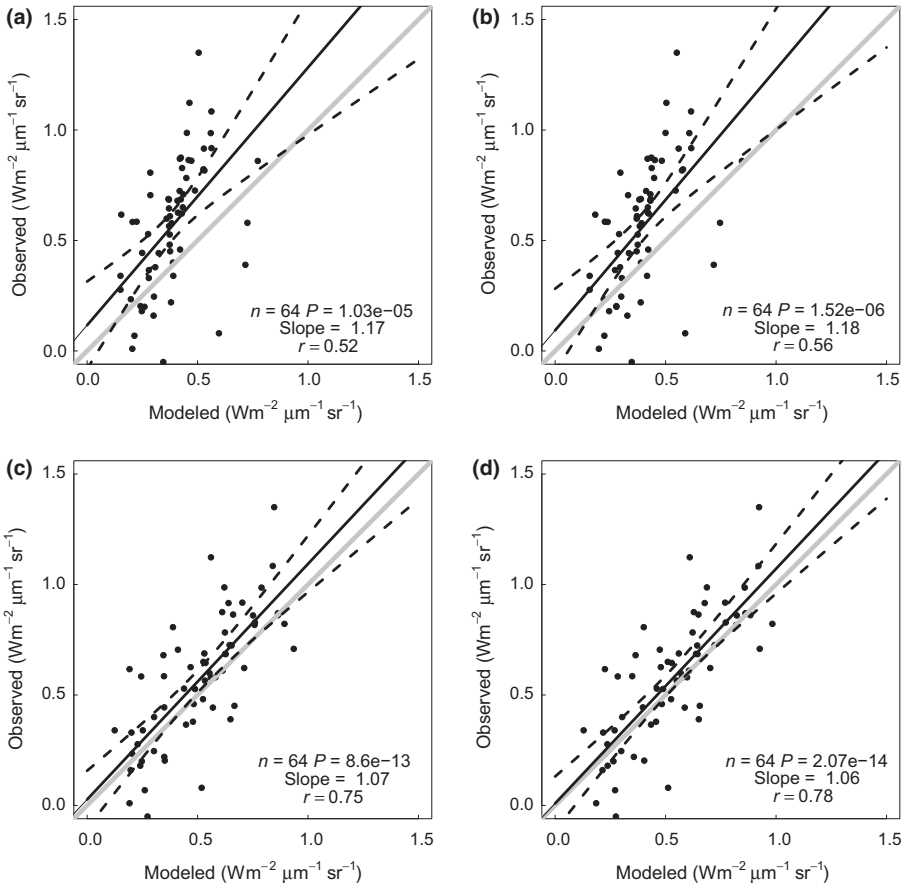

Fig. 2 Scatterplot of modeled vs observed fluorescence emission at 760 nm (F_{760}) for the runs (a) Reference, (b) Traits, (c) Structure and (d) Traits–Structure. Runs with variable structural parameters between treatments show the best model performances (c, d), as evidenced by the linear relationship (black solid line) being closer to the 1: 1 line (gray solid line) and having larger Pearson's correlation coefficient values (*r*).

due to the overestimation of GPP by SCOPE. The linear relationship between F_{760} and LAI improves substantially for the Run Traits–Structure. The analysis of covariance (ANCOVA) shows that there are no significant differences in the slope and intercept of the linear relationship F_{760}–LAI between observations and Run Traits–Structure ($P = 0.181$).

© 2017 The Authors
New Phytologist © 2017 New Phytologist Trust

Table 3 Evaluation of the performance of the fluorescence emission at 760 nm (F_{760}) of the different model runs ($n = 64$)

	r	MAE	RMSE	R^2	Slope	EF
Reference	0.52	0.26	0.31	0.27	1.17	−0.10
Traits	0.56	0.25	0.30	0.31	1.18	−0.01
Structure	0.75	0.16	0.21	0.56	1.07	0.52
Traits–Structure	0.78	0.15	0.19	0.61	1.06	0.59

r, Pearson's correlation coefficient; MAE, mean absolute error; R^2, determination coefficient; slope, parameter of the linear regression between observed and modeled data (Fig. 2); EF, modeling efficiency. All of the statistics are computed according to Janssen & Heuberger (1995).

Figure 6 reports the relationship between observed GPP and observed F_{760} for each treatment (Fig. 6a), the relationship between observed GPP and F_{760} modeled with the Run Traits–Structure (Fig. 6b), and both GPP and F_{760} modeled (Fig 6c). Figure 6(a) shows the observed slopes of the relationship GPP–F_{760} for each treatment; in particular the NP treatment differentiates from the others. Figure 6(b,c) show that with the Run Traits–Structure we are able to reproduce the change in the GPP–F_{760} slopes between treatments.

The prediction of nutrient treatment effects on the GPP–F_{760} relationship clearly improved by using the Run Traits–Structure (Fig. 7). The largest step in improvement was achieved by letting the LIDFa and LIDFb vary with treatment, whereas the additional variation of *C*ab and V_{cmax} yielded a further but smaller improvement.

Discussion

Our understanding of the mechanisms controlling the spatio-temporal variability of SIF, and its use as a proxy for GPP is still limited (Porcar-Castell *et al.*, 2014; Damm *et al.*, 2015; Rascher *et al.*, 2015). The present contribution reports on a nutrient fertilization experiment where observational and modeling approaches are combined to improve the understanding of the F_{760} drivers. This includes how changes in structural properties and functional traits induced by nitrogen (N) and phosphorus (P) treatments affect temporal and within-treatment variability of the SIF at 760 nm (F_{760}) signal, and the GPP–F_{760} relationship.

Effects of fertilization-induced changes in structural and functional traits on the F_{760} signal

The physiological changes induced by fertilization, in particular N, lead to an increase in photosynthetic capacity under high light conditions and water availability (Fig. 1). The fertilization leads to the expected changes in N% and P%, and also to a variation in plant forms across treatments (Fig. 1; Table 2). For more discussion, refer to Perez-Priego *et al.* (2015).

Measured F_{760} shows a clear difference between treatments during the peak of the growing season, after the fertilization, as well as late in the season. The increase in F_{760} with N fertilization is the consequence of higher N% in plants, and as consequence of an increased leaf area index (LAI) (Fig. 1), chlorophyll *a*+*b* (*C*ab) content and maximum carboxylation capacity (V_{cmax}) observed in this study but also in other grassland studies (Feng & Dietze, 2013; Walker *et al.*, 2014). This leads to an increase of fluorescence emission at 760 nm as aconsequence of *C*ab increase and also an adjustment of the ratio between nonphotochemical quenching (NPQ) activity and fluorescence signal as a consequence of relieved N limitation (Cendrero-Mateo *et al.*, 2016). By considering the variability in functional traits induced by fertilization into the parameterization of the soil–canopy observation of photosynthesis and energy model (SCOPE) model we obtain an improvement of the description of the spatial (i.e. among treatments at the same sampling date, Fig 3a) and temporal variability of F_{760} (Fig. 2; Table 3).

In the present study it is shown that both changes in functional traits and in canopy structure (changes of the leaf inclination distribution function LIDFa (average) and LIDFb (bimodality) as a result of changed plant form abundances) substantially control the spatial (among treatments) and temporal variability in F_{760}. In the literature, sensitivity analyses of SCOPE show that theLAI,

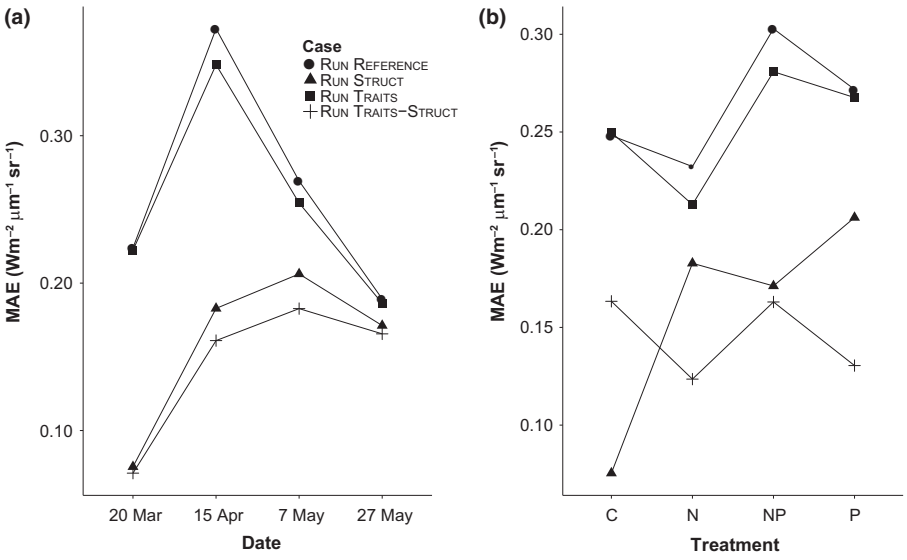

Fig. 3 Mean absolute deviation (MAE) of fluorescence emission at 760 nm (F_{760}) for the different model runs computed by (a) campaigns and (b) treatment. The error is reduced most by letting structural parameters vary across treatments. The impact of variable functional traits is evident after the fertilization (15 April onward).

© 2017 The Authors
New Phytologist © 2017 New Phytologist Trust

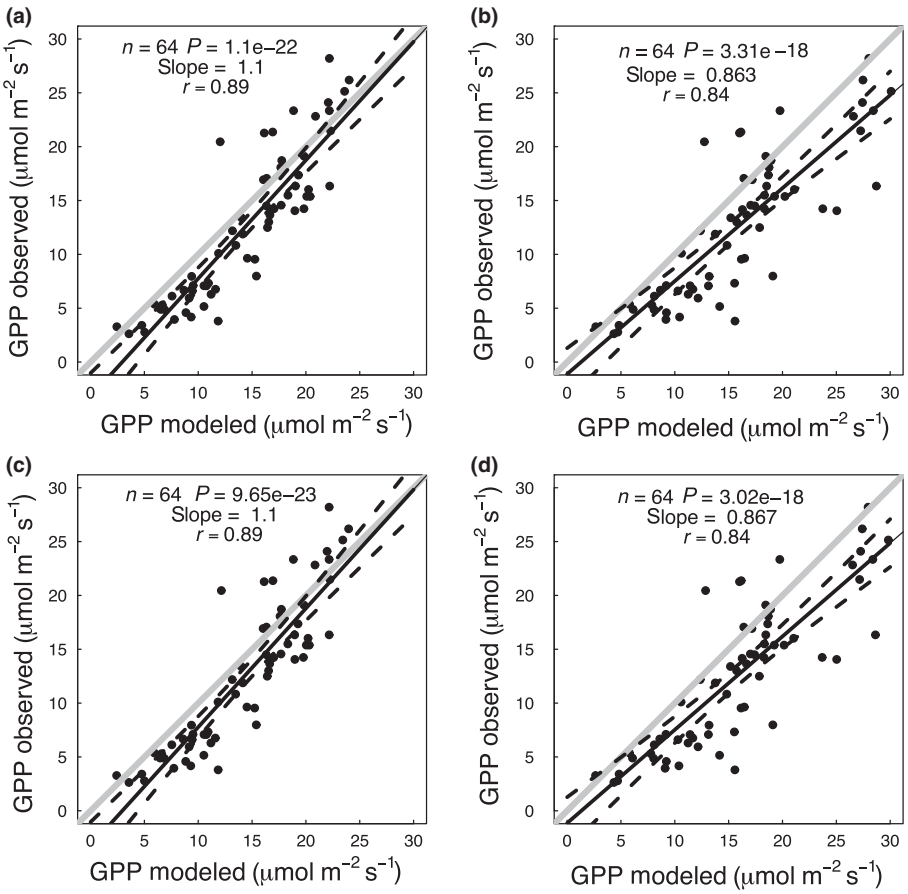

Fig. 4 Scatterplot of modeled vs observed gross primary productivity (GPP) for the runs (a) Reference, (b) Traits, (c) Structure and (d) Traits–Structure. The solid straight lines represent the linear regression between observed and modeled data; the gray lines represent the 1 : 1 line; the curvilinear dashed lines represent the 95% confidence interval.

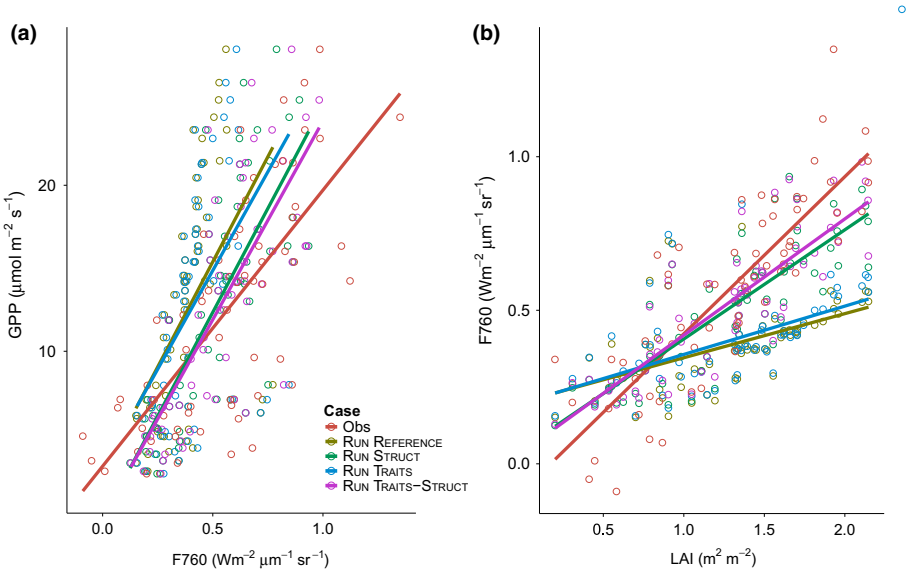

Fig. 5 Relationship between (a) gross primary productivity (GPP) and fluorescence emission at 760 nm (F_{760}) and (b) F_{760} and leaf area index (LAI). Different colors represent different model runs and the observations (red). ANCOVA shows statistically significant differences ($P < 0.01$) between the different slopes of the F_{760}–LAI relationship. No statistical significant differences were found between observation and the run and Traits–Structure ($P = 0.181$).

green: dry biomass ratio (C_{dm} and C_s) and LIDF parameters are important factors controlling the observed fluorescence emission (Damm *et al.*, 2015; Verrelst *et al.*, 2015, 2016; Rossini *et al.*, 2016). In this study we demonstrate that accounting for the changes in LIDF parameters resulting from the changes in plant form abundances after the treatment (Table 2) improves the description of F_{760}, and strongly reduces the bias between model and observations. The experimental design presented in this study cannot provide information to disentangle the contribution of plant competition or selective grazing to changes in plant form abundances after the treatment. Further studies that use grazing exclusion cages are needed to evaluate the importance of these two contrasting processes to variation in canopy structure.

© 2017 The Authors
New Phytologist © 2017 New Phytologist Trust

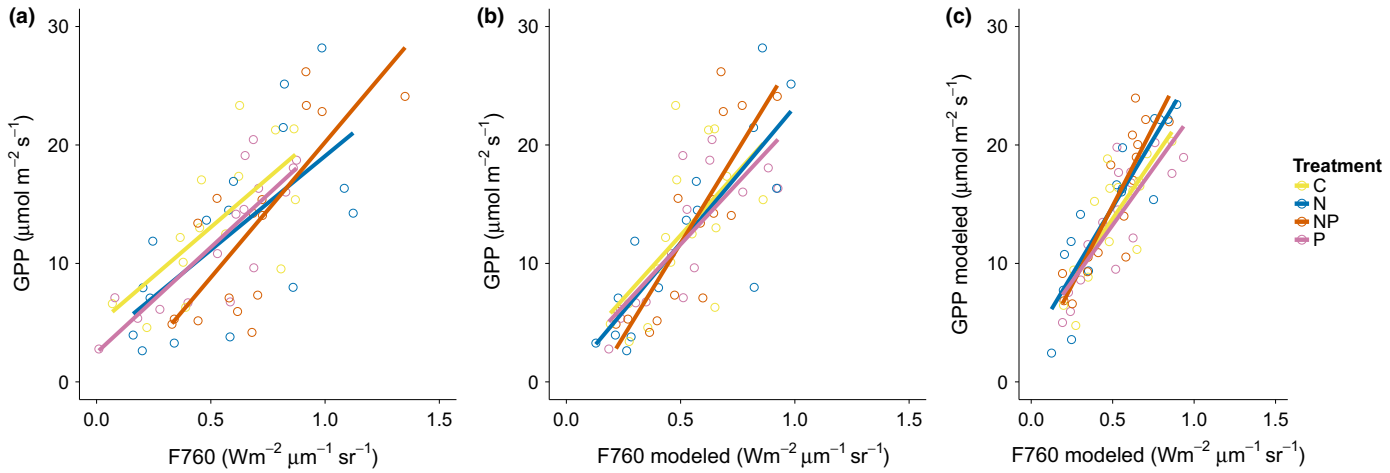

Fig. 6 Relationship between gross primary productivity (GPP) and fluorescence emission at 760 nm (F_{760}), both observed (a), GPP measured and F_{760} modeled (b), both modeled (c). Different lines represent different treatments.

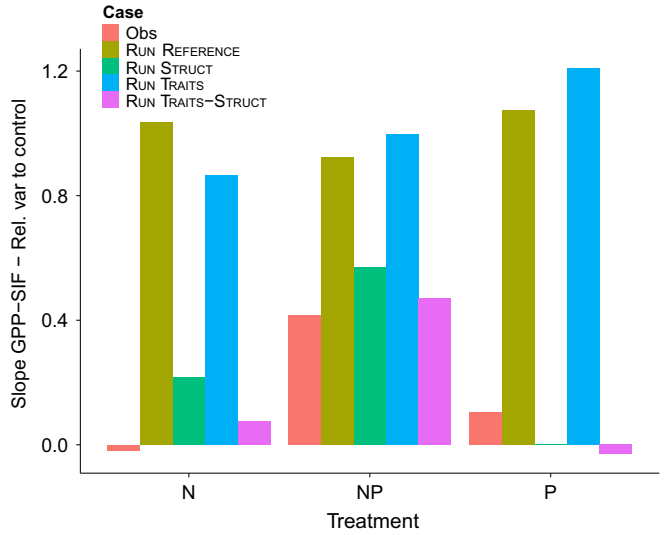

Fig. 7 Histogram reporting the change of the fluorescence emission at 760 nm vs gross primary productivity (F_{760}–GPP) slope under the nitrogen (N), phosphorus (P) and nitrogen–phosphorous (NP) addition treatments relative to the slope observed in the carbon (C) treatment. Different bars indicate different treatments.

Furthermore, when the spatio-temporal variability of functional traits, and more importantly canopy structure were accounted for, the SCOPE model made it possible to achieve a good description of the observed F_{760}, and of the slope between LAI and F_{760}. Finally, we show that in a grassland manipulated with nutrient addition, when LAI is prescribed, the *C*ab and LIDF parameters, and to a lesser extent V_{cmax} (Verrelst *et al.*, 2015), are responsible for the observed variability of F_{760}.

Drivers of GPP–F_{760} relationship and implications for light use efficiency modeling based on far-red SIF

Previous studies concluded that a better understanding of the effect of nutrient availability on the processes controlling the GPP–F_{760} relationship is needed to fully explore the possibilities offered by fluorescence retrieval to predict GPP (Perez-Priego *et al.*, 2015; Cendrero-Mateo *et al.*, 2016). These studies pointed out that variations in N% and P% in vegetation, in particular in conditions when N is limiting (Cendrero-Mateo *et al.*, 2016), might modulate the slope of the relationship GPP–F_{760}.

With the factorial modeling exercise presented in this study, we show that the observed GPP–F_{760} relationship is governed by a combination of changes in canopy structure (LIDF) and to a lesser extent to changes in functional traits (in particular V_{cmax}). Moreover, we show that with the proposed parameterization SCOPE is able to mimic the slope of GPP–F_{760} across treatments (Fig. 7), in particular for the combined nitrogen–phosphorus (NP) treatment.

According to Guanter *et al.* (2014), and updated by Damm *et al.* (2015), the relation between GPP and F_{760} can be simplified as:

$$GPP \approx F_{760} \cdot \frac{LUE_p}{f_{esc} \cdot LUE_f} \quad \text{Eqn 3}$$

(LUE_p, light use efficiency for photosynthesis; LUE_f, light use efficiency of fluorescence (i.e. fluorescence yield); f_{esc}, a parameter accounting for the structural interference determining the fraction of F_{760} photons that are escaping the canopy). The variable ratio of LUE_p: (LUE_f·f_{esc}) as a function of nutrient availability observed in this study contrasts with the assumption of a fixed ratio for coarse plant functional type, indicating that this assumption can result in significant error in GPP estimation if the spatio-temporal variability due to different nutrient availability is not considered. On the one hand, variations in the relationship between GPP and F_{760} may be related to physiological changes induced by fertilization (Cendrero-Mateo *et al.*, 2016) that determines changes in the LUE_p: LUE_f ratio. On the other, changes in canopy structure dependent on changes in the abundances of plant forms might control the parameter f_{esc}. Different canopy architectures and orientation of leaves with respect to the illumination angle play an important role in light absorption, probability of photons escaping the canopy (Knyazikhin *et al.*, 2013) and

© 2017 The Authors
New Phytologist © 2017 New Phytologist Trust

patterns of F_{760} emission, as demonstrated in Fig S5. Figure S5 (b) shows a lower F_{760} emission measured by the sensor in case of erectophile vegetation (i.e. grasses) compared with vegetation with planophile and spherical LIDF, under the same LAI, *C*ab, V_{cmax} and illumination conditions. In the case of planophile vegetation, a larger portion of the F_{760} is visible from a top view, whereas for vegetation with more vertically oriented leaves, much less can be seen directly from the top, even if the total emitted fluorescence is similar to that of vegetation with horizontal leaves. However, the leaf angle distribution does not affect GPP in the same way, which is controlled by absorbed photosynthetically active radiation (PAR) and functional traits (*C*ab and V_{cmax}). For this reason, in treatments characterized by a higher abundance of erectophile vegetation (e.g. NP in field campaigns 3 and 4; Table 2) the sensitivity of GPP to variations of F_{760} increases compared with plots characterized by vegetation with planophile and spherical LIDF. As a result, the slope of the relationship between GPP and F_{760} changes across treatments. Furthermore, the differences in canopy structure affecting multi-scattering and reabsorption need to be taken into account (Fig. S5g).

Focus on the fluorescence peak in the far-red (*c.* 740 nm) was a limitation in this study due the spectrometer used, which did not allow for good retrieval of the peak in the red region (*c.* 685 nm) (Julitta *et al.*, 2016). The fluorescence emission in the red peak stems mainly from photosystem II (PSII) activity, whereas the far-red peak is the combination of both photosystem I and II (PSI and PSII). Recently, many studies have suggested that the fluorescence of PSII is less affected by absorbed photosynthetically active radiation (APAR), and therefore provides more information on LUE (Porcar-Castell *et al.*, 2014; Rossini *et al.*, 2015, 2016). Future efforts should be focused on the improvement of field measurements of red and far-red fluorescence, and the impact of the use of this information as multiple constraint for radiative transfer model inversion. Selection of the FLuorescence EXplorer (FLEX) as an Earth Explorer 8 mission by the European Space Agency, should make available consistent global maps of red and far-red fluorescence as well as reflectance. Such information will offer an unique way to advance our understanding and quantification of biosphere dynamics.

The results of this study also point toward the use of SCOPE as a powerful tool for the understanding of the relationship between fluorescence emission and GPP, and disentanglement of the main drivers of this relationship using experimental studies. As shown in the present study, a combination of field studies and modeling could support the future development of a parameterization of semi-empirical light and fluorescence use efficiency models (Eqn 3), by identifying the main controlling factors of the ratio between LUE_p and LUE_f, as well as of f_{esc} for different canopy architectures (LAI, LIDF parameters) and environmental and physiological conditions (e.g. nutrient availability, functional traits). Considering a more mechanistic perspective, only a few studies in the literature have explored the possibility of deriving V_{cmax} from remote sensing data: Houborg *et al.* (2013) estimated V_{cmax} from an empirical relationship with *C*ab, the latter being derived from a radiative transfer model inversion using LANDSAT satellite data as a constraint; and Zhang *et al.* (2014) estimated V_{cmax} using SCOPE and satellite estimates of F_{760}. Both studies highlight the importance of estimating seasonal variables V_{cmax} and *C*ab to improve the simulation of GPP by terrestrial biosphere models (Koffi *et al.*, 2015). The results obtained in the present study for the simulation of GPP, F_{760} and their functional relationship suggest that SCOPE offers potential to derive functional traits (e.g. V_{cmax}, *C*ab) by inverting the model against multiple constraints (i.e. using fluorescence, reflectance, and CO_2 and water fluxes). This can open important perspectives for mapping functional traits and parameters of terrestrial biosphere models using satellite information such as SIF.

Acknowledgements

The authors acknowledge the Alexander von Humboldt Foundation for supporting this research with the Max-Planck Prize to Markus Reichstein, and the EUFAR TA project DEHESHyrE (EU FP7 Program). We acknowledge the Majadas de Tiétar city council for its support. The authors acknowledge the Freiland Group and in particular Martin Hertel from MPI-Jena and Ramón López-Jiménez (CEAM) for technical assistance. The authors thank the anonymous referee and the editor for their comments on the work, Alessandro Cescatti for discussions about the results and Silvana Schott for the graphics.

Author contributions

M.M., O.P-P., M. Rossini and M. Reichstein designed the analysis and carried out the majority of the data analysis; M.M., U.R. and M. Rossini designed the modeling exercise; M.M. and C.V.d.T. conducted the simulations with SCOPE; M.M. wrote the article; G.M., A. Berninger, V.B., A.C., F.F., J-H.G., K.H., E.J-A., T.J., O.K., T.S.E-M., T.W.H. and A.P-B. contributed to the data collection in the field, estimation of LAI and laboratory analysis; T.M., T.W.H. and S.Z. contributed in the discussion about the parameterization of functional traits; F.F., T.J., M.P.M., J.P-L. and A. Burkart contributed with the field calibration of the spectrometers and the discussion about fluorescence; and O.P-P. and T.W. developed the software for the computation of CO_2 fluxes from the chambers. All of the authors contributed to the discussion of the results and to the writing.

References

Barillot R, Louarn G, Escobar-Gutiérrez AJ, Huynh P, Combes D. 2011. How good is the turbid medium-based approach for accounting for light partitioning in contrasted grass–legume intercropping systems? *Annals of Botany* **108**: 1013–1024.

Beer C, Reichstein M, Tomelleri E, Ciais P, Jung M, Carvalhais N, Rodenbeck C, Arain MA, Baldocchi D, Bonan GB *et al.* 2010. Terrestrial gross carbon dioxide uptake: global distribution and covariation with climate. *Science* **329**: 834–838.

Byrd RH, Lu P, Nocedal J, Zhu C. 1995. A limited memory algorithm for bound constrained optimization. *SIAM Journal on Scientific Computing* **16**: 1190–1208.

Campbell GS, Norman JM. 1998. *An introduction to environmental biophysics.* New York, NY, USA: Springer.

© 2017 The Authors
New Phytologist © 2017 New Phytologist Trust

Cendrero-Mateo MP, Moran MS, Papuga SA, Thorp KR, Alonso L, Moreno J, Ponce-Campos G, Rascher U, Wang G. 2016. Plant chlorophyll fluorescence: active and passive measurements at canopy and leaf scales with different nitrogen treatments. *Journal of Experimental Botany* **67**: 275–286.

Cogliati S, Rossini M, Julitta T, Meroni M, Schickling A, Burkart A, Pinto F, Rascher U, Colombo R. 2015. Continuous and long-term measurements of reflectance and sun-induced chlorophyll fluorescence by using novel automated field spectroscopy systems. *Remote Sensing of Environment* **164**: 270–281.

Collatz GJ, Ball JT, Grivet C, Berry JA. 1991. Physiological and environmental regulation of stomatal conductance, photosynthesis and transpiration: a model that includes a laminar boundary layer. *Agricultural and Forest Meteorology* **54**: 107–136.

Collatz GJ, Ribas-Carbo M, Berry JA. 1992. Coupled photosynthesis-stomatal conductance model for leaves of C_4 plants. *Australian Journal of Plant Physiology* **19**: 519–538.

Damm A, Elber J, Erler A, Gioli B, Hamdi K, Hutjes R, Kosvancova M, Meroni M, Miglietta F, Moersch A *et al.* 2010. Remote sensing of sun-induced fluorescence to improve modeling of diurnal courses of gross primary production (GPP). *Global Change Biology* **16**: 171–186.

Damm A, Guanter L, Paul-Limoges E, van der Tol C, Hueni A, Buchmann N, Eugster W, Ammann C, Schaepman ME. 2015. Far-red sun-induced chlorophyll fluorescence shows ecosystem-specific relationships to gross primary production: an assessment based on observational and modeling approaches. *Remote Sensing of Environment* **166**: 91–105.

Feng X, Dietze M. 2013. Scale dependence in the effects of leaf ecophysiological traits on photosynthesis: Bayesian parameterization of photosynthesis models. *New Phytologist* **200**: 1132–1144.

Fournier A, Daumard F, Champagne S, Ounis A, Goulas Y, Moya I. 2012. Effect of canopy structure on sun-induced chlorophyll fluorescence. *ISPRS Journal of Photogrammetry and Remote Sensing* **68**: 112–120.

Guanter L, Frankenberg C, Dudhia A, Lewis PE, Gómez-Dans J, Kuze A, Suto H, Grainger RG. 2012. Retrieval and global assessment of terrestrial chlorophyll fluorescence from GOSAT space measurements. *Remote Sensing of Environment* **121**: 236–251.

Guanter L, Rossini M, Colombo R, Meroni M, Frankenberg C, Lee JE, Joiner J. 2013. Using field spectroscopy to assess the potential of statistical approaches for the retrieval of sun-induced chlorophyll fluorescence from ground and space. *Remote Sensing of Environment* **133**: 52–61.

Guanter L, Zhang Y, Jung M, Joiner J, Voigt M, Berry JA, Frankenberg C, Huete AR, Zarco-Tejada P, Lee JE *et al.* 2014. Global and time-resolved monitoring of crop photosynthesis with chlorophyll fluorescence. *Proceedings of the National Academy of Sciences, USA* **111**: E1327–E1333.

Heinsch FA, Zhao M, Running SW, Kimball JS, Nemani RR, Davis KJ, Bolstad PV, Cook BD, Desai AR, Ricciuto DM *et al.* 2006. Evaluation of remote sensing based terrestrial productivity from MODIS using regional tower eddy flux network observations. *IEEE Transactions on Geoscience and Remote Sensing* **44**: 1908–1923.

Houborg R, Cescatti A, Migliavacca M, Kustas WP. 2013. Satellite retrievals of leaf chlorophyll and photosynthetic capacity for improved modeling of GPP. *Agricultural and Forest Meteorology* **177**: 10–23.

Jacquemoud S, Baret F. 1990. PROSPECT: a model of leaf optical properties spectra. *Remote Sensing of Environment* **34**: 75–91.

Janssen PHM, Heuberger PSC. 1995. Calibration of process-oriented models. *Ecological Modelling* **83**: 55–66.

Julitta T, Corp LA, Rossini M, Burkart A, Cogliati S, Davies N, Hom M, Arthur AM, Middleton EM, Rascher U *et al.* 2016. Comparison of sun-induced chlorophyll fluorescence estimates obtained from four portable field spectroradiometers. *Remote Sensing* **8**: 122.

Jung M, Reichstein M, Margolis HA, Cescatti A, Richardson AD, Arain MA, Arneth A, Bernhofer C, Bonal D, Chen J *et al.* 2011. Global patterns of land-atmosphere fluxes of carbon dioxide, latent heat, and sensible heat derived from eddy covariance, satellite, and meteorological observations. *Journal of Geophysical Research – Biogeosciences* **116**: G00j07.

Knyazikhin Y, Schull MA, Stenberg P, Mõttus M, Rautiainen M, Yang Y, Marshak A, Carmona PL, Kaufmann RK, Lewis P *et al.* 2013. Hyperspectral remote sensing of foliar nitrogen content. *Proceedings of the National Academy of Sciences, USA* **110**: E185–E192.

Koffi EN, Rayner PJ, Norton AJ, Frankenberg C, Scholze M. 2015. Investigating the usefulness of satellite-derived fluorescence data in inferring gross primary productivity within the carbon cycle data assimilation system. *Biogeosciences* **12**: 4067–4084.

Lee JE, Frankenberg C, van der Tol C, Berry JA, Guanter L, Boyce CK, Fisher JB, Morrow E, Worden JR, Asefi S *et al.* 2013. Forest productivity and water stress in Amazonia: observations from GOSAT chlorophyll fluorescence. *Proceedings of the Royal Society B* **280**: 20130171.

Liu L, Guan L, Liu X. 2017. Directly estimating diurnal changes in GPP for C_3 and C_4 crops using far-red sun-induced chlorophyll fluorescence. *Agricultural and Forest Meteorology* **232**: 1–9.

Meroni M, Barducci A, Cogliati S, Castagnoli F, Rossini M, Busetto L, Migliavacca M, Cremonese E, Galvagno M, Colombo R *et al.* 2011. The hyperspectral irradiometer, a new instrument for long-term and unattended field spectroscopy measurements. *Review of Scientific Instruments* **82**: 043106.

Meroni M, Busetto L, Colombo R, Guanter L, Moreno J, Verhoef W. 2010. Performance of spectral fitting methods for vegetation fluorescence quantification. *Remote Sensing of Environment* **114**: 363–374.

Meroni M, Colombo R. 2009. 3S: a novel program for field spectroscopy. *Computers and Geosciences* **35**: 1491–1496.

Meroni M, Picchi V, Rossini M, Cogliati S, Panigada C, Nali C, Lorenzini G, Colombo R. 2008. Leaf level early assessment of ozone injuries by passive fluorescence and photochemical reflectance index. *International Journal of Remote Sensing* **29**: 5409–5422.

Meroni M, Rossini M, Guanter L, Alonso L, Rascher U, Colombo R, Moreno J. 2009. Remote sensing of solar-induced chlorophyll fluorescence: review of methods and applications. *Remote Sensing of Environment* **113**: 2037–2051.

Niinemets Ü, Kollist H, García-Plazaola JI, Hernández A, Becerril JM. 2003. Do the capacity and kinetics for modification of xanthophyll cycle pool size depend on growth irradiance in temperate trees? *Plant, Cell & Environment* **26**: 1787–1801.

Parazoo NC, Bowman K, Fisher JB, Frankenberg C, Jones DBA, Cescatti A, Pérez-Priego O, Wohlfahrt G, Montagnani L. 2014. Terrestrial gross primary production inferred from satellite fluorescence and vegetation models. *Global Change Biology* **20**: 3103–3121.

Perez-Priego O, Guan J, Rossini M, Fava F, Wutzler T, Moreno G, Carvalhais N, Carrara A, Kolle O, Julitta T *et al.* 2015. Sun-induced chlorophyll fluorescence and photochemical reflectance index improve remote-sensing gross primary production estimates under varying nutrient availability in a typical Mediterranean savanna ecosystem. *Biogeosciences* **12**: 6351–6367.

Porcar-Castell A, Tyystjarvi E, Atherton J, van der Tol C, Flexas J, Pfundel EE, Moreno J, Frankenberg C, Berry JA. 2014. Linking chlorophyll a fluorescence to photosynthesis for remote sensing applications: mechanisms and challenges. *Journal of Experimental Botany* **65**: 4065–4095.

Rascher U, Alonso L, Burkart A, Cilia C, Cogliati S, Colombo R, Damm A, Drusch M, Guanter L, Hanus J *et al.* 2015. Sun-induced fluorescence – a new probe of photosynthesis: first maps from the imaging spectrometer HyPlant. *Global Change Biology* **21**: 4673–4684.

Rossini M, Meroni M, Celesti M, Cogliati S, Julitta T, Panigada C, Rascher U, van der Tol C, Colombo R. 2016. Analysis of red and far-red sun-induced chlorophyll fluorescence and their ratio in different canopies based on observed and modeled data. *Remote Sensing* **8**: 412.

Rossini M, Meroni M, Migliavacca M, Manca G, Cogliati S, Busetto L, Picchi V, Cescatti A, Seufert G, Colombo R. 2010. High resolution field spectroscopy measurements for estimating gross ecosystem production in a rice field. *Agricultural and Forest Meteorology* **150**: 1283–1296.

Rossini M, Nedbal L, Guanter L, Ač A, Alonso L, Burkart A, Cogliati S, Colombo R, Damm A, Drusch M *et al.* 2015. Red and far red sun-induced chlorophyll fluorescence as a measure of plant photosynthesis. *Geophysical Research Letters* **42**: 1632–1639.

van der Tol C, Berry JA, Campbell PKE, Rascher U. 2014. Models of fluorescence and photosynthesis for interpreting measurements of solar-induced chlorophyll fluorescence. *Journal of Geophysical Research: Biogeosciences* **119**: 2312–2327.

van der Tol C, Berry JA, Campbell PKE, Rascher U. 2015. Models of fluorescence and photosynthesis for interpreting measurements of solar-induced

© 2017 The Authors
New Phytologist © 2017 New Phytologist Trust

chlorophyll fluorescence. *Journal of Geophysical Research: Biogeosciences* **119**: 2312–2327.

van der Tol C, Verhoef W, Rosema A. 2009a. A model for chlorophyll fluorescence and photosynthesis at leaf scale. *Agricultural and Forest Meteorology* **149**: 96–105.

van der Tol C, Verhoef W, Timmermans J, Verhoef A, Su Z. 2009b. An integrated model of soil-canopy spectral radiances, photosynthesis, fluorescence, temperature and energy balance. *Biogeosciences* **6**: 3109–3129.

Verhoef W. 1984. Light scattering by leaf layers with application to canopy reflectance modeling: the SAIL model. *Remote Sensing of Environment* **16**: 125–141.

Verrelst J, Rivera JP, van der Tol C, Magnani F, Mohammed G, Moreno J. 2015. Global sensitivity analysis of the SCOPE model: what drives simulated canopy-leaving sun-induced fluorescence? *Remote Sensing of Environment* **166**: 8–21.

Verrelst J, van der Tol C, Magnani F, Sabater N, Rivera JP, Mohammed G, Moreno J. 2016. Evaluating the predictive power of sun-induced chlorophyll fluorescence to estimate net photosynthesis of vegetation canopies: a SCOPE modeling study. *Remote Sensing of Environment* **176**: 139–151.

Vilfan N, van der Tol V, Muller O, Rascher U, Verhoef W. 2016. Fluspect-B: A model for leaf fluorescence, reflectance and transmittance spectra. *Remote Sensing of Environment* **186**: 596–615.

Walker AP, Beckerman AP, Gu L, Kattge J, Cernusak LA, Domingues TF, Scales JC, Wohlfahrt G, Wullschleger SD, Woodward FI. 2014. The relationship of leaf photosynthetic traits – V_{cmax} and J_{max} – to leaf nitrogen, leaf phosphorus, and specific leaf area: a meta-analysis and modeling study. *Ecology and Evolution* **4**: 3218–3235.

Wieneke S, Ahrends H, Damm A, Pinto F, Stadler A, Rossini M, Rascher U. 2016. Airborne based spectroscopy of red and far-red sun-induced chlorophyll fluorescence: implications for improved estimates of gross primary productivity. *Remote Sensing of Environment* **184**: 654–667.

Wohlfahrt G, Bahn M, Tappeiner U, Cernusca A. 2001. A multi-component, multi-species model of vegetation–atmosphere CO_2 and energy exchange for mountain grasslands. *Agricultural and Forest Meteorology* **106**: 261–287.

Yang X, Tang J, Mustard JF, Lee J-E, Rossini M, Joiner J, Munger JW, Kornfeld A, Richardson AD. 2015. Solar-induced chlorophyll fluorescence that correlates with canopy photosynthesis on diurnal and seasonal scales in a temperate deciduous forest. *Geophysical Research Letters* **42**: 2977–2987.

Zhang Y, Guanter L, Berry JA, Joiner J, van der Tol C, Huete A, Gitelson A, Voigt M, Kohler P. 2014. Estimation of vegetation photosynthetic capacity from space-based measurements of chlorophyll fluorescence for terrestrial biosphere models. *Global Change Biology* **20**: 3727–3742.

Zhang Y, Xiao X, Jin C, Dong J, Zhou S, Wagle P, Joiner J, Guanter L, Zhang Y, Zhang G *et al.* 2016. Consistency between sun-induced chlorophyll fluorescence and gross primary production of vegetation in North America. *Remote Sensing of Environment* **183**: 154–169.

Supporting Information

Additional Supporting Information may be found online in the Supporting Information tab for this article:

Fig. S1 Aerial photograph of the experimental site (SMANIE).

Fig. S2 Schematic representation of the assumptions behind the factorial modeling exercise performed in this study.

Fig. S3 Scatterplot modeled vs observed GPP and F_{760} for a run of SCOPE with a different assumption on the distribution of nitrogen in the green to dry component.

Fig. S4 Example of different leaf inclination distribution function (LIDF) for four types of canopy structures.

Fig. S5 Example of the sensitivity of reflectance and fluorescence to the assumption on leaf inclination distribution function.

Fig. S6 Scatterplot modeled vs observed normalized difference vegetation index for the different model runs.

Fig. S7 Canopy reflectance measured.

Fig. S8 Canopy reflectance modeled.

Fig. S9 Scatterplot modeled vs observed GPP and F_{760} for a run with SCOPE parameterized using the assumption of spherical leaf inclination distribution function.

Methods S1 Alternative methods to parameterize *C*ab and V_{cmax} and evaluation.

Please note: Wiley Blackwell are not responsible for the content or functionality of any Supporting Information supplied by the authors. Any queries (other than missing material) should be directed to the *New Phytologist* Central Office.

© 2017 The Authors
New Phytologist © 2017 New Phytologist Trust